



Energy, Mines and
Resources Canada

Énergie, Mines et
Ressources Canada

Earth Physics Branch

Direction de la physique du globe

1 Observatory Crescent
Ottawa Canada
K1A 0Y3

1 Place de l'Observatoire
Ottawa Canada
K1A 0Y3

**Geothermal Service
of Canada**

**Service géothermique
du Canada**

**MODELLING OF DEEP GROUNDWATER FLOW
IN SASKATCHEWAN**

**G. Garven and L.W. Vigrass
University of Regina
Regina, Saskatchewan
S4S 0A2**

**Earth Physics Branch Open File Number 85-17
Dossier public de la Direction de la Physique du Globe No. 85-17**

NOT FOR REPRODUCTION

**Department of Energy, Mines and
Resources Canada
Earth Physics Branch
Division of Gravity, Geothermics
and Geodynamics**

REPRODUCTION INTERDITE

**Ministre de l'Énergie, des Mines
et des Ressources du Canada
Direction de la physique du globe
Division de la gravité, géothermie
et géodynamique**

ABSTRACT

The finite element method has been used to model numerically the hydrodynamics of the Williston structural basin along three transects of the basin.

The numerical results show that surface topography and extent of salt beds are important controls on the flow patterns. Cross formational flow is especially important near the downdip edge of regional salt beds. Flow rates are quite low (0.5 m/year) even when quite high permeabilities are assumed for the lower Paleozoic section. Nevertheless, the flow rates are able to perturb the temperature field that results from conductive heat flow.

The temperature perturbations resulting from fluid flow have important implications for geothermal energy applications and also influence maturation of petroleum source beds. The results have important implications for petroleum migration, genesis of salt solution structures, and several other practical problems.

RÉSUMÉ

L'hydrodynamique du bassin structural de Williston a été modélisé le long de trois transects par la méthode numérique d'éléments finis. Les résultats démontrent que la topographie à la surface et l'étendue des lits de sel sont des contrôles importants sur la configuration de l'écoulement. L'écoulement oblique dans les formations est surtout important près de l'extrémité en aval-pendage des lits de sel régionaux. Le débit est très bas (0.5 m/année) même si des perméabilités assez élevées sont prises pour le Paléozoïque inférieur. Cependant le débit peut perturber le champ thermique provenant du flux de chaleur par conductivité.

Ces perturbations thermiques sont d'une grande portée pour les applications en énergie géothermique et elles influencent aussi la maturation de la roche mère. L'importance des résultats pour la migration d'hydrocarbures, pour la genèse des structures de sel par dissolution et pour d'autres problèmes pratiques est marquée.

MODELLING OF DEEP GROUNDWATER FLOW
IN SASKATCHEWAN

Prepared for:

Energy, Mines and Resources Canada
Earth Physics Branch
Ottawa, Canada

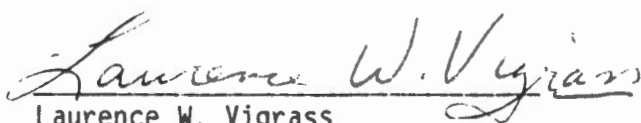
Under

DSS Contract OST 84-00069

Report Prepared by

G. Garven
and
L.W. Vigrass

Approved


Laurence W. Vigrass
Principal Investigator

Date: April 12, 1985

Contribution No. 121
Energy Research Unit
University of Regina
March, 1985

TABLE OF CONTENTS

	<u>Page</u>
List of Tables -----	ii
List of accompanying illustrations -----	iii
SUMMARY -----	v
INTRODUCTION -----	1
PART 1: GENERAL PROBLEM -----	3
Objectives -----	3
Work done -----	4
Results -----	5
Future work -----	6
PART 2: MODELLING RESULTS -----	8
Physics of flow and heat transport -----	8
Numerical formulation -----	14
Numerical results -----	20
SUMMARY AND CONCLUSIONS -----	26
References -----	27

LIST OF TABLES

Table

1	Standard model parameters -----	21
---	---------------------------------	----

LIST OF ACCOMPANYING ILLUSTRATIONS

PART 1

Fig.

- A Williston basin, Isopach and Structure Map
- B Williston Basin Area, General Topography
- C SASKW - General geology, well control, topographic names and TDS in formation waters
- D SASKC - General geology, well control, topographic names and TDS in formation waters
- E SASKE - General geology, well control, topographic names and TDS in formation waters

PART 2

(Each figure consists of a finite element mesh, hydraulic heads, velocity vectors, and temperatures).

- 1. SASKW: Standard model parameters (SMP).
- 2. SASKC: Standard model parameters (SMP).
- 3. SASKE: Standard model parameters (SMP).
- 4. SASKC1: $K_2 = 50$ (Winnipeg-Duperow hydraulic conductivity $K = \text{SMP} \times 10$).
- 5. SASKC2: $K_6 = 70$, $K_7 = 5$ (Mannville $K = \text{SMP} \times 3.5$; Cret. Shale $K = \text{SMP} \times 5$).
- 6. SASKC3: $K_{xx}/K_{zz} = 50$ ($\text{SMP} \times 0.5$).
- 7. SASKC4: $K_1 = 300$; Basal Heat Flux = 70mW/m^2 (Deadwood $K = \text{SMP} \times 3$; Basal Heat Flux = $\text{SMP} \times 1.17$)

8. SASKC5: $K_1 = 600$, $K_2 = 30$
(Deadwood $K = \text{SMP} \times 6$; Winnipeg-Duperow
 $K = \text{SMP} \times 6$; Basal Heat Flux = SMP)
9. SASKW5: Parameters as Fig. 8.
10. SASKC6: $K_7 = 3$; $K_3 = 10^{-5}$ isotropic, thermal
conductivities = $\text{SMP} \times 0.75$; (Cret. Shale K
= $\text{SMP} \times 3$, Prairie Salt $K = 10^{-5}$ but
isotropic).

SUMMARY

The finite element method has been used to model numerically the hydrodynamics of the Williston structural basin along three transects of the basin. The theoretical model approach has been used because we can use it to assess quantitatively the effects of regional groundwater movement on subsurface heat transport. Model parameters used in 1984-1985 are based on limited field data and the literature.

The numerical results show that surface topography and extent of salt beds are important controls on the flow patterns. Cross formational flow is especially important near the downdip edge of regional salt beds. Flow rates are quite low (0.5m/year) even when quite high permeabilities are assumed for the lower Paleozoic section. Nevertheless, the flow rates are able to perturb the temperature field that results from conductive heat flow. The perturbation is greatest when the hydraulic conductivity of the Tertiary-Cretaceous strata is considered to be large and when hydraulic anisotropy is considered to be low.

The temperature perturbations resulting from fluid flow have important implications for geothermal energy applications and also influence maturation of petroleum source beds. The results have important implications for petroleum migration, genesis of salt solution structures, and several other practical problems. Work should be continued in 1985-1986 to insure that the model parameters are realistic, to verify the model by field observations, to interpret the effects on geothermal and other applications, and to improve the model.

MODELLING OF DEEP GROUNDWATER FLOW
IN SASKATCHEWAN

INTRODUCTION

We have used the finite element method to model numerically the hydrodynamics of the Williston structural basin along three vertical transects of the basin. Earlier studies had shown that subsurface temperatures are strongly influenced by water movement. Most of the earlier studies are local in extent and qualitative in nature. The theoretical model approach was used because with it we can assess quantitatively the effects of regional groundwater movement on subsurface heat transport.

The results show that the topography and distribution of salt beds are important controls on deep groundwater flow. Cross formational flow is expected, influenced both by the topography and the distribution of salt. Overall flow rates within the basin are low even when we assume quite large permeabilities. Temperature perturbations resulting from the water flow are most obvious if we make the permeability of Tertiary-Cretaceous strata quite large and assume that hydraulic anisotropy is low.

The results have important implications for geothermal energy applications in sedimentary basins. The temperature distribution is also important because it influences maturation of petroleum source beds. The results have other important implications for petroleum migration, genesis of salt solution structures, sedimentary rock diagenesis, ore deposits, and environment.

The results obtained in 1985-1986 are based on model parameters based on limited field data and the literature. Work should be continued to insure that these parameters are realistic, to verify the model by field observations, to interpret the effects on geothermal, petroleum and other applications, and to improve the model.

The Introduction and Part 1 of this report were written by Vigrass. The modelling work was done by Garven who also prepared Part 2 and the Summary and Conclusions. Most of the geological work and preparation of the geological cross sections was done by Greg McTavish.

PART 1: GENERAL PROBLEM

Objectives

Overall and long-term objectives of the project are:

- 1) Determine the present regional, intermediate and local water flow patterns within the aquifer/aquitard complex that comprises the fill of the western Canadian basin.
- 2) Adjust the reservoir parameters and relate the present flow patterns to causative mechanisms (topography, thermal convection, water density effects resulting from salt solution).
- 3) Investigate past flow patterns and the effects of compaction.
- 4) Show how past and present flow patterns are related to:
 - a) generation, migration, accumulation and entrapment of petroleum;
 - b) distribution of temperature in the basin;
 - c) salt solution features;
 - d) chemistry of water and rock-water interactions;
 - e) potential sedimentary ore deposits;
 - f) flooding hazards in deep mines;
 - g) problems of storage and subsurface disposal.
- 5) Transfer the knowledge and techniques to other scientists and technologists.

The objectives for 1984-1985 were:

- 1) To determine how regional and local water flow patterns in deep subsurface beds affect temperature distribution in Saskatchewan.
- 2) To investigate and attempt to document vertical (cross-formational) flow.
- 3) To attempt to document fluid flow patterns along solution-derived edges of salt beds.

Work Done

1. Three regional geological cross sections were prepared using data from 100 deep wells in Saskatchewan, Manitoba, Montana, North Dakota and South Dakota. Locations for the three sections (SASKW - 960 km, SASKC - 900 km, SASKE - 1110 km) are shown relative to Williston Basin structure and isopachs in Figure A. The sections extend from areas of exposed Precambrian rocks (respectively Bearpaw Mountains, Little Rocky Mountains, and Black Hills) to the edge of sedimentary cover along the Precambrian Shield. There is a decrease in topographic elevation from 1,800 m AMSL in the south or southwest to 400 m AMSL or less in the north or northeast (Fig. B).

The three regional geological sections from classical "recharge" areas to classical "discharge" areas were plotted originally on a scale of 1:3,937 vertical and 1:236,220 horizontal (vertical exaggeration 60 X). Shown on these sections were stratigraphy (formations), known porous intervals, and some test data. Subsequently these sections were reduced in two stages: first, to about 1/4 scale (1:15,000 vertical) so that the sections were of manageable size; second at the CALCOMP

graphics stage, they were reduced to about 1:20,000 vertical. The cross sections are shown in this report at a scale that varies from about 1:40,000 vertical to 1:52,000 vertical (Figs. C, D, E, 1 to 10).

2. Theoretical models for the basin cross sections were developed utilizing the finite element method, the computer program developed by Garven, and hydrological-thermal parameters based on limited field data and the literature. Part 2 of this report is concerned with the modelling methods and the preliminary results from a sensitivity analysis.

3. The topographic features, well control, and main geological elements were transferred manually to Figures C, D and E. Also plotted were preliminary values for total dissolved solids in formation waters along the three basin cross sections (Figs. C, D, E).

It should be noted that we have only begun to adjust geohydrological parameters to detailed field observations and to compare the model results to observations of pressure and temperature in the basin.

Results

The numerical results are given in Part 2 and are shown graphically in Figures 1 - 10.

The numerical results show that the configuration of the water table (surface topography) and the presence or absence of salt beds are important controls on the sub-regional flow systems. Cross-formational flow is expected, especially near the downdip edge of regional salt

beds. Overall, the flow rates within the basin are low (0.5 m per year or less) even when quite high permeabilities are assumed for the older rocks. The flow rates are able to perturb the temperature field that results from conductive heat flow. This perturbation is greatest when the hydraulic conductivity of the Tertiary-Cretaceous strata is considered to be large and where hydraulic anisotropy is considered to be low. The temperature perturbation is not particularly sensitive to increased permeability of the lower Paleozoic beds.

Plotting of the total dissolved solids along the profiles in the Canadian portions of the basin (Figs. C, D, E) suggests a shift of the highly saline bubble away from the main recharge areas and toward the main discharge areas.

Future Work

The results confirm earlier qualitative work that indicates that subsurface temperatures in sedimentary basins are strongly influenced by water movement (see, for example, Majorowicz and Jessop, 1981). The resultant perturbations of temperature have a strong influence on geothermal energy applications and also influence maturation of petroleum source beds. In addition, the results have important implications for petroleum migration and accumulation and for the genesis of salt solution structures which determine the areal distribution of some petroleum pools. Several other important practical problems in sediment diagenesis, ore deposits, and environment are related to movement of deep subsurface waters.

Because of the potential economic importance of the modelling work, it should be continued. We are recommending a continuation of the 1984-85 studies in several areas:

1. Gathering and analyses of field data that will result in realistic models. The type of data required are on water table distribution, permeabilities, porosities, fluid salinity and density, and thermal properties.

2. Gathering and analysis of field data that will confirm the predicted deep groundwater movement patterns. Observations are necessary on subsurface pressures, temperatures, water chemistry, and salt solution history.

3. Interpretation and assessment of the results as these affect geothermal applications, source rock maturity, petroleum accumulations, and other areas.

4. Improvements in the computer-mathematical modelling so that we can use shorter sections with closely defined boundary conditions.

5. Transfer of the results at a suitable time to other scientists and technologists.

PART 2: MODELLING RESULTS

The purpose of this part of the report is to present some theoretical models for the basin hydrodynamics and to assess quantitatively the effects of regional groundwater flow on subsurface heat transport. We have utilized the finite element method to numerically solve the coupled equations of fluid flow and thermal energy conservation in two-dimensional section representations of the basin. The paragraphs below describe the mathematical model, numerical approach, and preliminary results from a sensitivity analysis.

Physics of Fluid Flow and Heat Transport

In a compacted sedimentary basin, fluid flow is driven by regional gradients in the hydraulic potential set up by the configuration of the water table. For moderate climates the water table generally conforms to the land surface topography. The hydraulic potential represents the potential energy per unit mass of fluid, and therefore its value will decrease from points of higher elevation on the water table to points at lower elevation. Below the water table (saturated zone) the hydraulic potential can be related to a hydraulic head h as

$$h = \frac{\phi}{g} \quad (1)$$

which represents the energy per unit weight of fluid, where g is the acceleration due to gravity. The hydraulic head is formally defined by

$$h = \frac{p}{\rho_0 g} + z \quad (2)$$

where p is gauge pressure, ρ_0 is a reference fluid density, and z is the elevation of the point above a reference datum. Head can be directly measured in shallow groundwater flow systems as the water level in completed wells or piezometers, but in deep sedimentary basins it is computed from drill-stem test measurements of fluid pressure. Spatial measurements or predictions of h or ϕ define the potential field from which flow patterns and rates can be calculated (Freeze and Cherry, 1979). Note from the definition of head that $h = z$ on the water-table surface, and therefore flow across a sedimentary basin will always be from areas of higher topographic elevation to areas of lower elevations. The exact nature of the flow paths depends on the water-table configuration and subsurface geology (Toth, 1962; Freeze and Witherspoon, 1967). Variations in fluid density, caused by temperature and salinity gradients, also modify flow patterns in deep groundwater flow systems (Garven, 1982).

Rates of flow through porous media are commonly presented as the Darcy velocity (discharge per unit area of porous media) or specific discharge, \bar{q} , and as the average linear velocity (discharge per unit area of pore space), \bar{v} . The two flow velocities are related via

$$\bar{v} = \bar{q}/\phi \quad (2.5)$$

where ϕ is the porosity of the medium. The specific discharge vector is given by the generalized Darcy equation

$$\bar{q} = \frac{-k}{\mu} (\nabla p + \rho g \nabla z) \quad (3)$$

where \underline{k} is the intrinsic permeability tensor and μ is the viscosity of water. We have chosen to rewrite (3) in terms of the fresh-water hydraulic head h and the hydraulic conductivity K :

$$\overline{q} = -\underline{K}\underline{\mu}_r (\nabla h + \rho_r \nabla z) \quad (4)$$

where

$$\underline{K} = \frac{\underline{k} \rho_0 g}{\mu_0} \quad (5)$$

$$\underline{\mu}_r = \frac{\mu_0}{\mu} \quad (6)$$

and

$$\rho_r = \frac{\rho - \rho_0}{\rho_0} \quad (7)$$

Here ρ_0 and μ_0 are the fluid density and viscosity at a specified reference temperature, salinity, and pressure. Equation (4) identifies the two driving forces causing fluid flow, hydraulic-head gradients created by the relief on the water table, and a buoyancy-head gradient created by spatial differences in density. The full form of the hydraulic conductivity tensor in the x-z plane is given by

$$\underline{K} = \begin{bmatrix} K_{xx} & K_{xz} \\ K_{zx} & K_{zz} \end{bmatrix} \quad (8)$$

In the case where the coordinates axes are aligned with the principal directions of permeability, the off diagonal terms in (8) became zero, and therefore only the "horizontal" and "vertical" hydraulic conductivities need to be specified for a given stratigraphic unit.

Regional groundwater flow in a compacted sedimentary basin can be treated as being at steady state, provided the configuration of the water table remains nearly constant and that changes in water-table elevation are small compared to the total thickness of the stratigraphic pile (Freeze and Cherry, 1979). Under steady conditions, recharge balances discharge across the basin, and the equation of fluid mass conservation is given by (Bear, 1972):

$$\nabla \cdot (\rho \bar{q}) = 0 \quad (9)$$

Substituting (4) into (9) gives the final form of our governing equation of flow:

$$\nabla \cdot [K_{\mu r} (\nabla h + \rho_r \nabla Z)] = 0 \quad (10)$$

Equation (10) fully describes inhomogeneous, steady groundwater flow in heterogeneous and anisotropic, rigid porous media. With the specification of boundary conditions, fluid properties, and hydraulic conductivities, the hydraulic head field is determined by solving (10), and flow rates can then be calculated at all (x,z) from (4).

Transport of heat in a sedimentary basin occurs through conduction, convection, and thermal dispersion. The conductive heat flux J_c can be written using Fourier's equation:

$$J_c = -\underline{\underline{k}} \nabla T \quad (11)$$

where κ is the effective thermal conductivity of the saturated porous media. Normally the thermal conductivity is written as a scalar quantity which is some function of the conductivity of the fluid and solid phases. We have used the relationship:

$$\kappa = \kappa_f \phi + \kappa_s (1-\phi). \quad (12)$$

Thermal dispersion represents the transport of heat through mechanical mixing of the fluid along the tortuous flow path, which is caused by heterogeneities in the porous media that have not been specifically modelled in the continuum representation of the flow field. The thermal dispersion flux J_D is given as:

$$\underline{J}_D = -\phi \underline{D}_H \nabla T \quad (13)$$

where D_H is the thermal dispersion tensor (Smith and Chapman, 1983; Garven, 1982). In practice, the effects of conduction and thermal dispersion cannot be separated, and thus the effective conduction-dispersion coefficient E is defined by:

$$\underline{E} = \kappa + \phi \underline{D}_H \quad (14)$$

Assuming steady-state heat flow (Domenico and Palciauskas, 1973), the equation of conservation of thermal energy can be derived by combining the conduction-dispersion and convection effects, and the result gives:

$$\nabla \cdot (\underline{E} \nabla T) - \rho c \bar{q} \cdot \nabla T = 0 \quad (15)$$

where T is the temperature and c is the specific heat of the fluid. This form of the heat equation assumes thermal equilibrium between fluid and rock. The first term in (15) represents the net heat flux by conduction-dispersion, and the second term accounts for the heat flux due to convection in the fluid flow system. Prescribing thermal properties and fluid flow rates, along with boundary conditions, allows for the solution of $T(x,z)$.

Equations (4), (10), and (15) define the mathematical model for steady fluid flow and heat transport in a compacted sedimentary basin, subjected to topography-induced hydraulic gradients created by the regional slope in the water table. Because of the physical coupling between the temperature-dependent density and viscosity, and the presence of the convection term, the equations ought to be solved simultaneously. In addition, equations of state for fluid density and viscosity must be specified. We have employed:

$$\rho = \rho(p, T, S)$$

and

$$\mu = \mu(p, T, S)$$

(16)

where S is the fluid salinity, expressed as an equivalent weight percent of NaCl in the water (Garven, 1982).

Numerical Formulation of the Transport Equations

The governing equations are solved numerically by using a Galerkin-based finite-element technique with linear basis functions applied over triangular elements. The finite element method is well suited to modelling flow in large basins because of its ability in easily handling complex geometries on the boundaries and tensorial properties of the media. Details regarding the application of finite elements to groundwater flow and transport are given in Pinder and Gray (1977). We will only give a brief review of the method as used in our modelling of the Williston basin and adjoining area.

The region of flow is first subdivided into a set of finite elements, with the corners of the elements represented by nodal coordinates in the (x,z) plane. The size and shape of the elements are arbitrary, but generally the finite element mesh is made fine enough to model complicated boundaries and lithology changes. A finer mesh is also desirable for those parts of the flow field where steep gradients in head or temperature are expected. The accuracy of the numerical solution increases with the number of elements used in discretizing the flow region, but limitations do exist in terms of computer storage memory and simulation costs for central processing unit time.

Assuming we seek an approximate solution to the flow equation (10), let the trial solution be of the form:

$$h \approx \hat{h} = \sum_{m=1}^N h_m \xi_m^e \quad (17)$$

where h = hydraulic head (exact solution)
 \hat{h} = approximate hydraulic-head solution
 N = total number of nodes in mesh
 m = nodal index
 h_m = hydraulic head coefficient (unknown)
 ξ_m^e = local basis function
 e = element index

The coefficients h_m are computed to satisfy boundary conditions and the necessary requirement of orthogonality, namely

$$\sum_e \iint_{R^e} L(\hat{h}) \xi_n^e dR^e = 0 \quad n = 1, 2, \dots, N \quad (18)$$

where the operator $L(\hat{h})$ is given by

$$L(\hat{h}) = \nabla \cdot [\underline{k} \rho \mu_r (\nabla \hat{h} + \rho_r \nabla z)] \quad (19)$$

The N integral equations defined in (18) represent the element contributions over the local areas R^e which together comprise the total region R . The local basis ξ_n^e functions are chosen here to be linear across the e element, varying from a value of unity at node n and zero at other nodes. For triangular elements, the basis functions are

$$\xi_n^e = \frac{1}{2\Delta^e} (a_n + b_n x + c_n z) \quad (20)$$

in which Δ^e is the element area, and the geometric coefficients a_n , b_n , and c_n are calculated from the local nodal coordinates as:

$$\begin{aligned} b_1 &= z_1 - z_3 & c_1 &= x_3 - x_2 \\ b_2 &= z_3 - z_1 & c_2 &= x_1 - x_3 \\ b_3 &= z_1 - z_2 & c_3 &= x_2 - x_1 \end{aligned} \quad (21)$$

and

$$2\Delta = b_1 c_2 - c_1 b_2$$

Here the points (x_1, x_2, x_3) and (z_1, z_2, z_3) are the local coordinates for nodes $n=1, 2, 3$ in the triangle. Note that the derivatives of the basis functions are also easily expressed in terms of the expressions in (21).

Application of Green's first identity to the set of integral equations of (18) results in a new set of equations given by:

$$A_{nm} \cdot h_m + B_n = Q_n \quad (22)$$

where A_{nm} is an $N \times N$ matrix, and B_n and Q_n are vectors of size N . Terms in the conductance or stiffness matrix A are:

$$\begin{aligned} A_{nm} &= \sum_e \iint_{Re} \underline{K} \rho \mu_r \nabla \xi_n^e \cdot \nabla \xi_m^e dR \\ &= \sum_e \frac{\rho \mu_r}{4\Delta} [K_{xx} b_n b_m + K_{xz} (c_n b_m + b_m c_m) + K_{zz} c_n c_m] \end{aligned} \quad (23)$$

and the buoyancy vector B ,

$$B_n = \sum_e \iint_{Re} \underline{K} \rho \mu_r \nabla Z \cdot \nabla \xi_n^e dR^e$$

$$= \sum_e \frac{\rho \mu_r \rho_r}{2} (K_{xz} b_n + K_{zz} c_n) \quad (24)$$

and the lateral flux vector Q_n ,

$$Q_n = - \sum_e \int_r q \xi_n^e d\Gamma = - \sum_e \frac{q \cdot L^e}{2} \quad (25)$$

In (25), r signifies an element boundary, L^e is the length of the element side experiencing a flow rate q .

The system of equations (22) is solved directly for the unknown heads h_m using Gaussian elimination. The symmetric and banded nature of the conductance matrix is taken advantage of in the solution process. With the hydraulic head gradients in hand, Darcy velocities are calculated for each element from (4), which can be recast in terms of the basis functions and head coefficients as:

$$q_x^e = - \sum_{m=1}^3 \left(K_{xx} \mu_r \frac{b_m}{2\Delta} h_m + K_{xz} \mu_r \frac{c_m}{2\Delta} h_m + K_{xz} \frac{\mu_r \rho_r}{3} \right) \quad (26)$$

$$q_z^e = - \sum_{m=1}^3 \left(K_{zx} \mu_r \frac{b_m}{2\Delta} + K_{zz} \mu_r \frac{c_m}{2\Delta} + K_{zz} \frac{\mu_r \rho_r}{3} \right)$$

These vectors are stored for later use in solving the heat transport equation.

Once again an approximate solution is sought in the form of a trial solution.

$$T \approx \hat{T} = \sum_{m=1}^N T_m \xi_m^e \quad (27)$$

where ξ_m^e are the same basis functions given in (20), and T_m are temperature coefficients for the nodal grid. Setting the residual resulting from the approximation of T by \hat{T} orthogonal to the N basis functions results in another set of integral equations,

$$\sum_e \iint_{Re} L(\hat{T}) \cdot \xi_n^e dR^e = 0 \quad n = 1, 2, \dots, N \quad (28)$$

where

$$L(\hat{T}) = \nabla \cdot (\underline{E} \nabla T) - \rho c \bar{q} \cdot \nabla T \quad (29)$$

Performing the substitutions results in new matrix equation:

$$S_{nm} \cdot T_m = F_n \quad (30)$$

where S_{nm} is an $N \times N$ matrix and F_n is a vector of size N . The thermal conductance matrix S is given by

$$S_{nm} = \sum_e \iint_{Re} [\underline{E} \nabla \xi_n^e \cdot \nabla \xi_m^e + \rho c \bar{q} \xi_n^e \cdot \nabla \xi_m^e] dR^e$$

$$= \sum_e \left[\frac{1}{4\Delta} (E_{xx} b_n b_m + E_{xz} (b_n c_m + c_n c_m) + E_{zz} c_n c_m) + \frac{\rho c}{6} (q_x b_m + q_z c_m) \right] \quad (31)$$

This matrix is also banded, but it is asymmetric due to the convection terms. The lateral flux vector F_n becomes

$$F_n = -\sum_e \int_{\Gamma^e} J \cdot \xi_n^e d\Gamma^e = -\sum_e \frac{J \cdot L^e}{2} \quad (32)$$

where L^e is the length of the element side experiencing a heat flux J . As in the case of fluid flow (25), this vector is zero at interior nodes in the grid and on no flow (insulated) boundaries.

In our numerical code, the fluid flow equation (22) is solved first, with an initial guess for density and viscosity, then the Darcy velocities are incorporated into solving the heat transport equation (30). With new values of temperature, fluid properties are evaluated from the state equations (16), and an updated set of heads and velocities are obtained for solving the heat equation. This iterative procedure is repeated until the maximum change in temperature between iterations converges to less than a tolerance level of 1°C for all nodes in the mesh. For the types of simulations presented here, convergence is generally achieved after several iterations. The FORTRAN-based code then utilizes CALCOMP type graphics subroutines for displaying the numerical results. Model output consists of the plotted mesh, contoured fresh-water hydraulic heads, average-linear velocity vectors, and contoured temperatures.

Numerical Results

Simulation results for the three hydrogeologic sections are shown in various figures discussed below. Note that the vertical scale of the sections are exaggerated by a factor of 60:1. Model parameter data were chosen from available field data and a variety of literature sources, such as Garven and Freeze (1984a, 1984b), Majorowicz and Jessop (1981), Toth (1978), and Hitchon (1968). Default values of the parameters are listed in Table I.

Boundary conditions are the same for all three of the hydrogeologic sections. The bottom boundary (Figures 1-3) conforms to the Precambrian-Paleozoic unconformity over most of the basin, except near the edges of the basin where the mesh has been extended into the crystalline basement in order to model flow in the deformed portion of the section at the extreme "left" side and in the feather-edge portion of the section at the extreme "right" side of the diagram. This boundary is impermeable to fluid flow, but it sustains a constant heat flux $J=60\text{mW/m}^2$ over the entire length. The top surface of the model represents the water table, along which the head is equal to the elevation at a given point. It is assumed to mimic the topography, and its position is in a state of dynamic equilibrium such that recharge balances discharge across the surface over reasonably long periods of time. The water table is prescribed as a constant temperature of 5°C , reflecting a slightly higher than average annual temperature for this region. Because it is a constant temperature, the net heat flux by forced convection will be zero across the water table. The left and right lateral sides of the model represent physical divides which are barriers to fluid and heat flow.

TABLE 1: Standard model parameters

WEST SASKATCHEWAN SECTION: SASKW

	<u>K_{xx}</u>	<u>Porosity</u>	
Cretaceous Shale	*K ₉ = 1 m/yr	n = 0.15	Anisotropy Ratio = $\frac{K_{xx}}{K_{zz}} = 100$
Mannville	K ₈ = 20	n = 0.30	Thermal Conductivity: Shale 2.0 W/m°C
Jurassic	K ₇ = 5	n = 0.10	Carbonate & Sands 3.0 W/m°C
Birdbear-Miss.	K ₆ = 5	n = 0.15	Evaporite 5.0 W/m°C
Dawson-Duperow	K ₅ = 5	n = 0.10	Specific Heat of Fluid: 4187 J/Kg°C
Elk Point	K ₄ = 10 ⁻⁵	n = 0.02	Thermal Dispersivities: 1 m
Winnipeg-Red River	K ₃ = 5	n = 0.10	Basal Heat Flux: 60 mW/m ² (1.5 H.F.U.)
Deadwood	K ₂ = 100	n = 0.20	Surface Temperature: 5°C
Precambrian	K ₁ = 10 ⁻⁵	n = 0.05	

CENTRAL SASKATCHEWAN SECTION: SASKC

Cretaceous Shale	K ₇ = 1 m/yr	n = 0.15	Anisotropy Ratio = $\frac{K_{xx}}{K_{zz}} = 100$
Mannville	K ₆ = 20	n = 0.30	Thermal Conductivity: Shale 2.0 W/m°C
Jurassic	K ₅ = 5	n = 0.10	Carbonate & Sands 3.0 W/m°C
Birdbear-Miss.	K ₄ = 10	n = 0.15	Evaporite 5.0 W/m°C
Elk Point	K ₃ = 10 ⁻⁵	n = 0.05	Specific Heat of Fluid: 4187 J/Kg°C
Winnipeg-Duperow	K ₂ = 5	n = 0.10	Thermal Dispersivities: 1 m
Deadwood	K ₁ = 100	n = 0.20	Basal Heat Flux: 60 mW/m ² (1.5 H.F.U.)
Precambrian	(same as K ₃)	n = 0.05	Surface Temperature: 5°C

EAST SASKATCHEWAN SECTION: SASKE

Cretaceous Shale	K ₉ = 1 m/yr	n = 0.15	Anisotropy Ratio = $\frac{K_{xx}}{K_{zz}} = 100$
Mannville	K ₈ = 20	n = 0.30	Thermal Conductivity: Shale 2.0 W/m°C
Jurassic-Triassic	K ₇ = 5	n = 0.10	Carbonate & Sands 3.0 W/m°C
Permian	K ₆ = 5	n = 0.10	Evaporite 5.0 W/m°C
Pennsylvanian	K ₅ = 15	n = 0.20	Specific Heat of Fluid: 4187 J/Kg°C
Birdbear - Miss.	K ₄ = 10	n = 0.15	Thermal Dispersivities: 1 m
Elk Point	K ₃ = 10 ⁻⁵	n = 0.05	Basal Heat Flux: 60 mW/m ² (1.5 H.F.U.)
Winnipeg-Duperow	K ₂ = 5	n = 0.10	Surface Temperature: 5°C
Deadwood	K ₁ = 100	n = 0.20	
Precambrian	(same as K ₃)		

[*Note: 1000 md ≈ 300 m/yr = 10⁻³ cm/s]

Figure 1: SASKW

This hydrogeologic section traverses some 960 km northward from the Bearpaw Mountains, across the Cypress Hills, and north to the edge of the Phanerozoic cover. Topography exerts the dominant control on the geometry of the flow system, despite the marked contrast in hydraulic conductivity between the stratigraphic layers. The uplands of the Bearpaw and Cypress Hills provide focal points for downward flow, whereas the Milk River, South and North Saskatchewan Rivers provide points for upward discharge of groundwater. These topographic effects are felt throughout the entire thickness of the sedimentary cover. Hydraulic head data have been contoured on 25-m contour interval, and temperatures have been contoured on a 5°C interval. The sharp discontinuity in the head contours near the center of the plot reflects the low permeability salt beds. Flow velocities (Darcy flux) reach a maximum of 0.4 m/yr in the Deadwood Fm. near the Bearpaw Mountains, and attain an average of about 0.08 m/yr near the basin center. The temperature map is largely conduction controlled, because of the small fluid flow rates. The isotherms mimic the topography, although they are greatly distorted due to the vertical exaggeration.

Figure 2: SASKC

Of the three sections, SASKC probably best reflects the hydrodynamic picture because of its orientation with topography of the basin. For the parameter data of Table I, topography again dominates the flow region by dissecting the basin into at least three sub-basin flow systems. Wood Mountain and the Little Rocky Mountains exert major control on recharge areas. Due to the thinner nature of the Deadwood

unit, less fluid is transported through this basal aquifer compared to Figure 1. One interesting feature that is visible is the significant cross-formational flow near the down-dip edge of the Elk Point salt. Flow is upward and toward the topographic low of Last Mountain Lake. As in the previous model an arbitrary linear salinity gradient is assumed to exist in the basin. In this simulation the salinity reaches a maximum of 18% equivalent weight NaCl at the deepest point in the section. No attempt has been made to input actual spatial variations in salinity at this stage of the modelling exercise.

Figure 3: SASKE

The eastern section extends almost 1100 km from the Black Hills northeasterly across the thickest part of the Williston basin. The hydraulic effect of the Devonian evaporites and increasing salinity with depth (maximum of 40% NaCl at the deepest point) are well delineated by the hydraulic head contours. Flow rates are a maximum at 1.7 m/yr in the Cambrian near the Black Hills, but are less than 0.05 m/yr in the same unit just north of the international border. Flow rates of 0.1 m/yr are predicted in the Deadwood sandstones below Duck Mountain. Temperatures attain a maximum of a 150°C at the thickest part of the section

Figure 4: SASKC1

The central section was chosen for a sensitivity analysis, and this figure shows one example where the horizontal hydraulic conductivity of the Winnipeg-Duperow hydrostratigraphic unit has been increased to 50 m/yr. As shown by the velocity vectors, the nature of the topography-

driven flow is depicted well. Flow rates increase substantially at the outcrop area near the basin margins, and rates of 0.2 m/yr occur in this unit in the basin interior. The effect of convection is still subdued, despite the greater permeability.

Figure 5: SASKC2

In this simulation, the horizontal hydraulic conductivities of the Mannville and Cretaceous shales were increased to values of 70 m/yr and 5 m/yr, respectively. The higher permeabilities allow for greater cross formational flow driven by the topographic effect. The result is a marked increase in vertical heat flux by convection as shown by the increased distortion of the isotherms, particularly in those parts of the basin experiencing upward discharge toward topographic lows. This is most pronounced near the low associated with Last Mountain Lake and the down-dip edge of the Elk Point salts. Under these condition, regional flow rates through the Deadwood approach 0.25 m/yr around the basin center.

Figure 6: SASKC3

To further evaluate the importance of cross formational flow, the overall hydraulic anisotropy of the basin strata was decreased from 100:1 to 50:1. These high anisotropy ratios are probably reasonable, considering the actual stratigraphic heterogeneities of the basin strata which we are ignoring because of the scale of the modelling. The lower anisotropy ratio permits greater vertical flow, which significantly perturbs the conductive heat flow gradient in groundwater discharge and recharge areas.

Figure 7: SASKC4

For this simulation, the hydraulic conductivity of Deadwood Fm. was increased to 300 m/yr (1 Darcy) and the basal heat flux increased to 70 mW/m². Higher flow rates create more modification of the temperature field.

Figure 8: SASKC5

Same as above, except the hydraulic conductivities of K₁ and K₂ are increased by a factor of six above those of Figure 4. Heat flow is greatly affected in the elevated, recharge part of the basin, but somewhat less so in the local discharge zones toward the basin margin. The 2.0 Darcy (600 m/yr) permeability for the Deadwood Fm. permits flow rates of 0.75 m/yr at the deepest point in the section model.

Figure 9: SASKW5

Parameters are the same as Figure 8, except now for the Western cross section. Velocities are slightly less than the previous example because of the smaller topographic slope across the basin in this profile.

Figure 10: SASKC6

For this model, the thermal conductivities of all of the stratigraphic units have been reduced to 75% of their values in Table I. In addition, the hydraulic conductivity was increased to 3 m/yr for the Cretaceous shales, and the Devonian salts are now assumed to be isotropic, with $K=10^{-5}$ m/yr in all directions. The lower thermal conductivity results in steeper thermal gradients, which enhance the effect of convection compared to the similar model of SASKC2 (Fig. 5).

SUMMARY AND CONCLUSIONS

1. Contemporary flow patterns and rates in the Williston basin are largely controlled by the water-table configuration which is a subdued replica of surface topography. The regional flow system geometry results in deeply-penetrating sub-regional flow systems, which breaks up any development of extensive, regionally continuous flow that could develop because of the hydrostratigraphy.
2. The low permeability of the Devonian salts presumably restricts the depth of the topographic effect in those areas underlain by salt. The models do predict extensive cross formational fluid flow due to the topography control, particularly near the down dip end of the salts.
3. Flow rates rarely exceed 0.5 m/yr in the central portions of the basin, even after assuming rather high permeabilities for the Lower Paleozoic section. Nevertheless, these flow rates are quite capable of perturbing the conductive heat flow in the recharge and discharge areas of the basin. Lowering the hydraulic anisotropy and increasing the post-Jurassic strata permeabilities enhances the visual effect of convective heat transport on subsurface temperature patterns.

References

- Bear, J. 1972, Dynamics of Fluids in Porous Media: New York, Am. Elsevier, 764 p.
- Domenico, P.A., and Palciauskas, V.V., 1973, Theoretical analysis of forced convective heat transfer in regional groundwater flow: Geol. Soc. America Bull., v. 84, p. 3803-3814.
- Freeze, R.A. and Cherry, J.A., 1979, Groundwater: Englewood Cliffs, N.J., Prentice Hall Inc., 604 p.
- Freeze, R.A. and Witherspoon, P.A., 1962, Theoretical analysis of regional groundwater flow: 2. Effect of water-table configuration and subsurface permeability variation: Water Resources Res., v. 3, p. 623-634.
- Garven, G., 1982, The role of groundwater flow in the genesis of stratabound ore deposits: A quantitative analysis: Ph.D. dissert., Univ. of British Columbia.
- Garven, G. and Freeze, R.A., 1984, Theoretical analysis of the role of groundwater flow in the genesis of stratabound ore deposits: 1. Mathematical and numerical model, 2. Quantitative results: Amer. Jour. Sci., v. 84, p. 1085-1174.
- Hitchon, B., 1968, Rock volume and pore volume data for plains region of western Canada sedimentary basin between latitudes 49° and 60°N: A.A.P.G. Bull., v. 52, p. 2318-2323.
- Majorowicz, J.A., and Jessop, A.M., 1981, Regional heat flow patterns in the western Canada sedimentary basin: Tectonophysics, v. 74, p. 209-238.
- Pinder, G.F., and Gray, W.G., 1977, Finite Element Simulation in Surface and Subsurface Hydrology: New York, Academic Press, 295 p.
- Smith, L., and Chapman, D.S., 1983, On the thermal effects of groundwater flow: 1. Regional scale systems: Jour. Geophys. Res., v. 88, p. 593-608.

- Toth, J. 1962, A theory of groundwater motion in small drainage basins in central Alberta: Jour. Geophys. Res., v. 67, p. 4375-4387
- Toth, J. 1978, Gravity-induced cross-formational flow of formational fluids, Red Earth region, Alberta, Canada: Analysis, patterns, and evolution: Water Resources Res., v. 14, p. 805-843.